J. Fluid Mech. (1975), *vol.* 67, *part* 1, *pp.* 125–143
Printed in Great Britain

Fine-structure turbulence in the wall region of a turbulent boundary layer

By H. UEDA

Department of Chemical Engineering, University of Kyoto, Japan

AND J. O. HINZE

Department of Mechanical Engineering,
University of Technology, Delft, Netherlands

(Received 15 October 1973 and in revised form 16 May 1974)

Measurements have been made concerning the fine structure of the turbulence in the part adjacent to the wall of the wall region of a plane turbulent boundary layer. The objective was to gain further information concerning the larger-scale disturbance mechanism which is mainly responsible for the generation of turbulence. Hot-wire anemometry was used and information on the fine structure was obtained by differentiating and filtering the hot-wire signal.

The distributions of the Kolmogorov microscale and of the flatness and skewness factors of the axial fluctuating velocity u and its first and second derivative determined at two Reynolds numbers suggest the existence of Reynolds number similarity. In the region $y^+ < 15$ the flatness and skewness factors of u increase with decreasing y^+. At approximately $y^+ = 15$ the flatness factor shows a minimum value, while the skewness factor becomes zero. This location agrees with that where the turbulence intensity u' has a maximum value. In the outer part of the wall region ($y^+ > 100$) the flatness and skewness factors approach values obtained in shear-free turbulence at the same turbulence Reynolds number.

The fine structure of the turbulence is strongly associated with and dominated by the random, larger-scale, intermittent inrush–ejection cycle. In the viscous sublayer both the fine structure, and the large-scale mechanism of the turbulence are influenced mainly by the inrush phase, while further out in the wall region ($y^+ > 40$) they are influenced by both inrush and ejection. As a result, in the viscous sublayer the average burst periods of the high frequency turbulence components and their flatness factors (of $\partial u/\partial t$ and of $\partial^2 u/\partial t^2$) attain values twice those in the outer part.

The change in the mechanism of the fine structure with distance from the wall is clearly demonstrated by the spectra of non-negative variables, i.e. $(\partial u/\partial t)^2$ and $(\partial^2 u/\partial t^2)^2$. The spectra agree with each other and decrease with increasing frequency, following a power law as predicted by Gurvich & Yaglom (1967). The power law applies to almost the whole frequency range, when the highest, viscous, frequency range is excluded. However, the exponent is different for the viscous sublayer and the outer part of the wall region. In the buffer layer the spectra have two distinct power-law regions. In the lower frequency

range the exponent is the same as that for the viscous sublayer, while in the higher frequency range it is the same as that for the outer part of the wall region.

---

1. Introduction

During the last decade visual studies have stimulated further research on the mechanism of the turbulence in the wall region, specifically on the disturbance mechanism and the turbulence production process. Kline *et al.* (1967), Kim, Kline & Reynolds (1971) and Corino & Brodkey (1969) observed that the disturbance mechanism consisted substantially of inrushes of fluid with high axial momentum into low momentum fluid near the wall alternating with ejections of low momentum fluid outward from the wall. As shown by Kim *et al.* (1971), Grass (1971), Willmarth & Lu (1972) and Wallace, Eckelmann & Brodkey (1972), the energy production process is strongly associated with and dominated by this intermittent inrush–ejection cycle, and consequently by the larger-scale turbulence.

It has long been known that locally in the wall region the turbulence energy production is almost of the same magnitude as the turbulence dissipation, which is mainly determined by the fine structure of the turbulence. As pointed out by Wallace *et al.* (1972), this turbulence dissipation process is also strongly related to the random and intermittent inrush–ejection cycle, because the region of the inrush and ejection events appears to correspond to the region of high local shear rates and consequently to high local dissipation of energy. Therefore, for a better understanding of the underlying disturbance mechanism, knowledge of the fine structure of the turbulence in the wall region is inevitably required. The present work is an effort to gain further information through detailed measurements of the fine structure of the turbulence near the wall in a plane turbulent boundary layer with zero pressure gradient. The measurements have been confined mostly to the inner part of the wall region, namely to

$$y^+ = yu^*/\nu < 500.$$

From measurements of the flatness factor of derivatives of the velocity fluctuations in grid-generated turbulence and in wake flows, Batchelor & Townsend (1949) first suggested that the fine structure of the turbulence tends to be locally concentrated, intermittent in nature and randomly scattered through the fluid in a rather spotty way. This has been confirmed by, amongst others, recent experiments in grid-generated turbulence by Kuo & Corrsin (1971, 1972). The same result has been obtained by Sandborn (1959) in a turbulent boundary layer. Experiments in the atmospheric boundary layer have been made by Pond & Stewart (1965), Gurvich & Yaglom (1967), Gibson, Stegen & Williams (1970), Van Atta & Chen (1970), Stewart, Wilson & Burling (1970), Sheih, Tennekes & Lumley (1971) and Wyngaard & Coté (1971). The results of all these experiments not only confirmed the intermittent nature of the fine structure of turbulence, but also showed that this intermittency increases with increasing turbulence

Reynolds number $Re_\lambda = u'\lambda_g/\nu$, where λ_g is the dissipation length scale corresponding to the transverse two-point velocity correlation (Hinze 1959, p. 36).

The degree of intermittency is closely related to the flatness factor of the probability density of a fluctuating signal, an increase in the intermittency corresponding to an increase in the flatness factor. From their measurements in grid-generated turbulence ($12 < Re_\lambda < 830$), Kuo & Corrsin (1971) obtained an empirical relation which shows the above increase of the flatness factor with Re_λ. They also showed that, for a fixed Re_λ, the flatness factor increased with decreasing characteristic length scale of the turbulence, i.e. with increasing wavenumber.

Important progress in the theory of the fine structure of turbulence has been made by Kolmogorov (1962), Oboukhov (1962) and Yaglom (1966). In addition to the original Kolmogorov (1941) hypotheses of local isotropy and similarity, Kolmogorov (1962) and Oboukhov (1962) further assumed that the logarithm of $\tilde{\epsilon}_r$, the average energy dissipation rate in a volume of linear dimension r, has a normal probability distribution. They obtained modified expressions for velocity structure functions. Later Yaglom (1966) and Gurvich & Yaglom (1967) showed, under the assumption of a cascade process for the breakdown of bigger to smaller eddies, that at large Reynolds number any non-negative quantity $a(x,t)$ governed by the fine structure of turbulence [e.g. $(\partial u/\partial x)^2$] has a lognormal probability distribution with the variance of $\ln \tilde{a}_r$ given by

$$\sigma_{\ln \tilde{a}_r} = A + \mu \ln (L/r). \tag{1}$$

Here L is an integral length scale, A depends on the characteristics of the large-scale motion, while μ is a universal constant. From the structure function of the energy dissipation a one-dimensional spectrum of $(\partial u/\partial x)^2$, or of ϵ, can be calculated:

$$E^{(1)}_{\epsilon\epsilon}(k) = B\overline{\epsilon^2} L(kL)^{\mu-1} \propto k^{\mu-1}. \tag{2}$$

Here k is the wavenumber, while Yaglom's notation is used (see §3.5).

Now Orszag (1970) showed that a lognormal probability distribution of $\tilde{\epsilon}$ leads to an inconsistency in the moments of various orders; they become indeterminate. However, for most of the values of the flatness factor (which is the fourth-order moment) obtained in the present investigation, this objection appears not to be serious (see Tennekes & Wyngaard 1972).

In accordance with the major objective, mentioned above, of the present experiments the distributions of characteristic length scales, flatness factors and skewness factors, and the variation of spectra of non-negative random variables with distance from the wall have been measured. We also wanted to clarify the fine structure of the turbulence in the wall region in the light of the above large-scale disturbance mechanism. And finally we wanted information concerning the degree of local isotropy of this fine structure.

2. Experimental equipment and procedure

The data reported here were taken in the turbulent boundary layer on a vertical Plexiglas wall placed at the centre-line of a low-speed low-turbulence wind tunnel. It was a tunnel of closed-circuit type with a rectangular test section

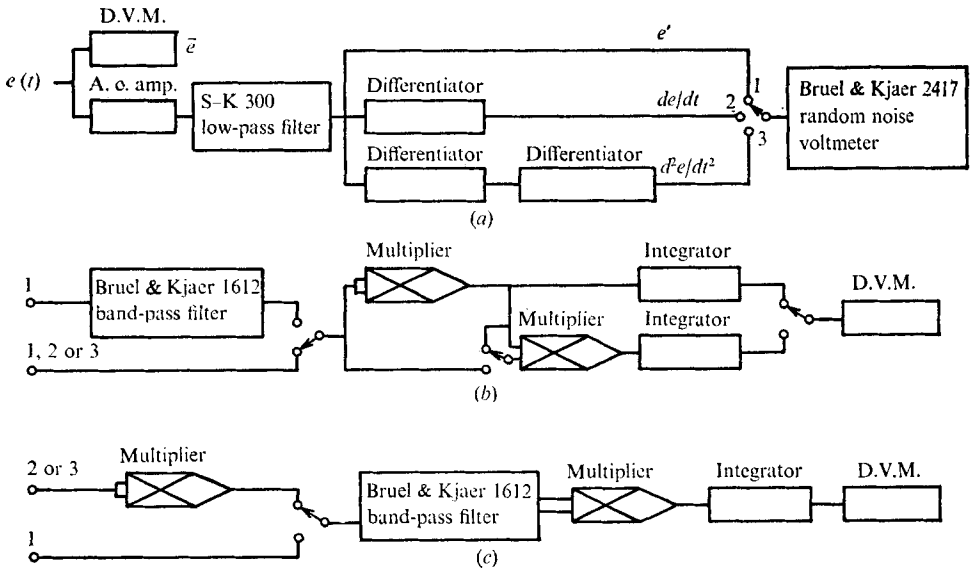

FIGURE 1. Block diagrams: (*a*) measurement of turbulence intensity and its first and second derivatives; (*b*) measurement of flatness and skewness factors; (*c*) spectrum analysis.

0·9 × 0·7 m, a 10:1 contraction and a turbulence level of about 0·03 % at a free-stream velocity of 13·5 m/s. The location of the transition to turbulent flow in the boundary layer was fixed by means of a tripping wire attached to the working surface about 3·38 m upstream of the test section. The longitudinal static-pressure gradient was adjusted to a negligibly small value by means of movable opposite walls. The data were obtained at the two free-stream velocities 4·10 and 13·5 m/s.

Only the longitudinal turbulent velocity component u was measured, with a single hot-wire anemometer set normal to the mean flow. The probe was made of jeweller's broaches spaced 10 mm apart and only a short central part of the wire (platinum wire 2 μm in diameter) was heated. The length of the heated part was 0·20 mm, which is equal to and three times the Kolmogorov microscale $\eta = (\nu^3/\epsilon)^{\frac{1}{4}}$ at the free-stream velocities of 4·10 and 13·5 m/s respectively. From Wyngaard's (1968) calculation based on Pao's (1965) spectrum, this length of the heated part was short enough so that spectral response to the first derivative of the fluctuating velocity was not significantly reduced by a length effect. A DISA Type 55M electronic unit for constant-temperature operation of the hot-wire anemometer was used in conjunction with a linearizer with an adjustable exponent. The hot wire was operated with an overheat ratio of 0·40. The conduction effect of the heated wire near the solid wall was sufficiently significant in the viscous sublayer to be taken into account, which was done using Wills' (1962) method.

Block diagrams of the electronic equipment used in this experiment are shown in figure 1. An a.c. amplifier (flat frequency response ranging from 0·3 to 40 000 Hz) was used to raise the linearized anemometer signal to a desired level

U_∞ (m/s)	$\delta_{0.99}$ (mm)	δ^* (mm)	θ (mm)	$H = \delta^*/\theta$	Re_δ	Re_θ	$\frac{1}{2}c_f$	u^* (m/s)
4·1	42·2	6·5	4·59	1·42	11450	1244	0·0019	0·18
13·5	39·7	6·8	4·75	1·43	35500	4248	0·0014	0·50

TABLE 1. Boundary-layer parameters for the experimental conditions

and to eliminate any d.c. level. Since the noise level of the compensated anemometer output increases linearly with frequency, a Spencer–Kennedy Model 300 filter was used to cut off the unwanted high frequency signal and noise.

The fine-structure turbulence signal was obtained by electronic differentiation and using a band-pass filter. Differentiation circuits with time constants stepwise variable from 0·0632 to $2{\cdot}083 \times 10^{-3}$ s and with a 18 db/octave cut-off at the high frequency end were used to obtain the first and the second derivatives. A Brüel & Kjaer Type 1612 band-pass filter set was used to obtain band-pass signals with various mid-band frequencies f_m and a relative bandwidth $\Delta f/f_m$ of 0·24.

For the measurements of flatness and skewness factors, two multipliers and two integrators were used (figure 1*b*). Calibration of the multipliers was made by feeding in a sine-wave signal. It was confirmed that the scaling factor

$$K = e_{\text{output}}/e^2_{\text{input}}$$

of the multipliers was constant within an error of 3% over the frequency range from 10 to 10000 Hz and over the input level from 0·5 to 5 V. Since the multipliers have lower and higher limits of input level, the measured values of flatness and skewness factors changed with the input level, especially when the signal had a very large flatness factor. Following Kuo & Corrsin (1971), the values at the horizontal parts of the curves of measured flatness and skewness factors *vs.* input level were taken as 'true' values.

3. Experimental results

3.1. *General flow specification*

The data reported here were obtained at the two air velocities 4·10 and 13·5 m/s. Table 1 gives the various boundary-layer parameters corresponding to these two velocities. The values of the friction velocity u^* were computed from the slope of the mean velocity profile near the wall, and obtained from both hot-wire anemometer and Pitot tube measurements. These values agree very well with those predicted by Ludwieg & Tillmann's (1949) empirical relation. The distributions of the mean velocity and the turbulence intensity are shown in figures 2 and 3, respectively. They are in fair agreement with those obtained in other investigations on flat-plate boundary layers and on pipe flows.

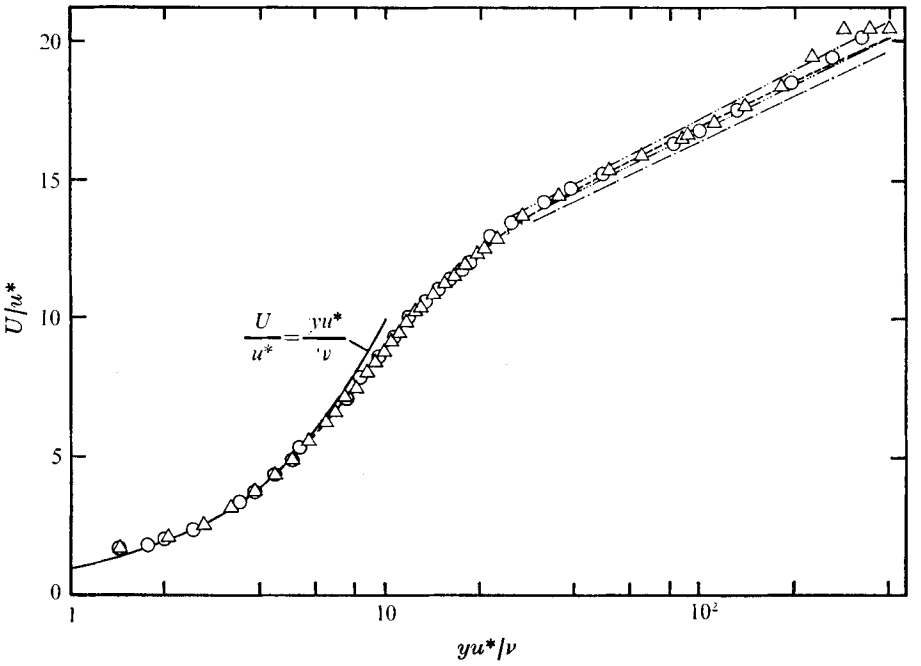

FIGURE 2. Distribution of mean velocity. Re_δ: △, 11450; ○, 35500. –·–·–, Nikuradse (1933); – –, Laufer (1954); – · –, Patel (1965); – · · –, Schlichting (1968, p. 565).

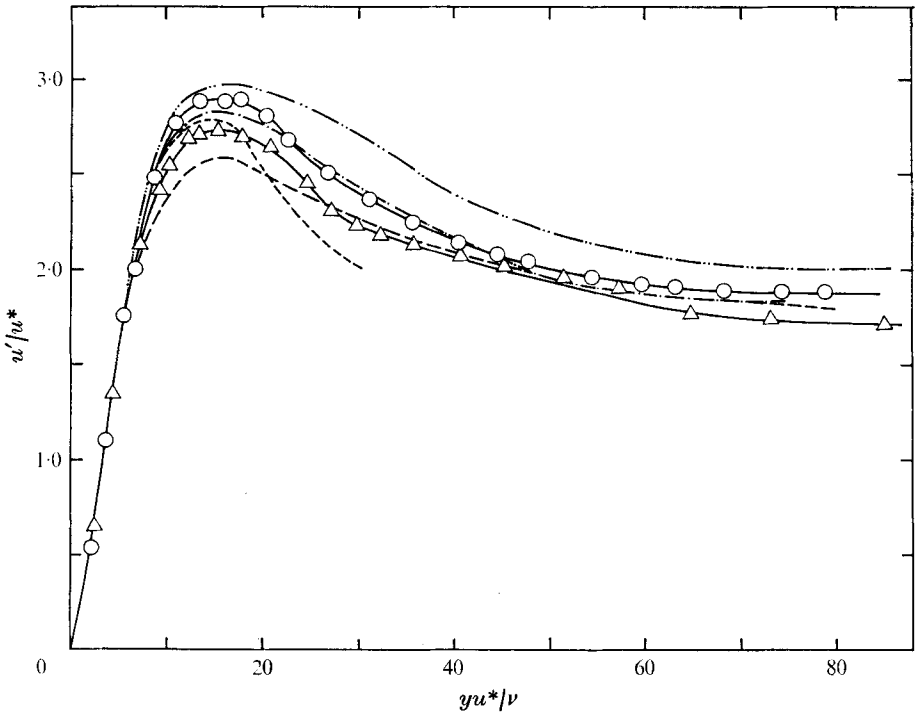

FIGURE 3. Distribution of turbulence intensity. Re_δ: △, 11450; ○, 35500. – – –, Laufer (1953), Re = 15300; – · · –, Morrison & Kronauer (1969), Re = 17000; – –, Eckelmann (1970), Re = 5600 and 82000; – · –, Grass (1971), Re = 6740.

3.2. *Distribution of length scales*

If the assumption of approximate homogeneity may be made concerning the fine structure of the turbulence that is responsible for the viscous dissipation, the general expression for the mean value of the dissipation, i.e.

$$\bar{\epsilon} = \nu \overline{\left(\frac{\partial u_i}{\partial x_j} + \frac{\partial u_j}{\partial x_i}\right) \frac{\partial u_i}{\partial x_j}}, \tag{3}$$

can be reduced to (see, for example, Hinze 1959, p. 66)

$$\bar{\epsilon} = \nu \overline{\frac{\partial u_i}{\partial x_j} \frac{\partial u_i}{\partial x_j}}. \tag{4}$$

The only possible effect of inhomogeneity on the calculation of $\bar{\epsilon}$ from (4) turns out to be an additional term $\nu \partial^2 \overline{v^2}/\partial y^2$ in the present case of a plane fully developed turbulent boundary layer. An estimate made from Laufer's (1954) data showed that the contribution of this term was less than a few per cent.

Experimental evidence shows that, except close to the wall, a further simplification can be made by assuming local isotropy (see, for example, Klebanoff 1955; Lawn 1971; Hinze 1973). The expression for $\bar{\epsilon}$ then takes on the well-known form

$$\bar{\epsilon} = 15\nu \overline{(\partial u/\partial x)^2} = 15\nu \overline{u^2}/\lambda_g^2. \tag{5}$$

Assuming Taylor's hypothesis of 'frozen' turbulence to be applicable to the fine structure, $\bar{\epsilon}$ has been determined by electronic differentiation of the hot-wire signal of u and by taking the mean-square value of the differentiated signal. From (5) the dissipation length scale λ_g is obtained. The Kolmogorov microscale η is obtained from

$$\eta = (\nu^3/\bar{\epsilon})^{\frac{1}{4}} = (15)^{-\frac{1}{4}} Re_\lambda^{-\frac{1}{2}} \lambda_g. \tag{6}$$

The distributions of $\lambda_g^+ = \lambda_g u^*/\nu$, $\eta^+ = \eta u^*/\nu$ and Re_λ as functions of y^+ are shown in figure 4, for the two Reynolds numbers $Re_\delta = 11450$ and 35500. There are some, but not marked, differences in the values for the two Reynolds numbers. Both λ_g^+ and Re_λ increase monotonically with distance from the wall only up to $y^+ \simeq 10$, and remain almost constant beyond this distance.

Since, for reasons mentioned above, the evaluation of $\bar{\epsilon}$ according to (5) cannot be correct close to the wall, the values of η^+ in the region $y^+ < 10$, say, must be considered with reserve. The same applies to the determination of λ_g^+ and Re_λ from (5).

3.3. *Flatness factor*

The flatness factor of a random variable $e(t)$ with normalized probability density $\mathscr{P}(e)$ is defined by

$$F(e) = \overline{e^4}/(\overline{e^2})^2 = \int_{-\infty}^{+\infty} de\, e^4 \mathscr{P}(e) \Big/ \left[\int_{-\infty}^{+\infty} de\, e^2 \mathscr{P}(e)\right]^2. \tag{7}$$

Since the fourth moment weights large values of e heavily, the flatness factor is a measure of the extent of the skirt of $\mathscr{P}(e)$. Thus a large value of F is obtained

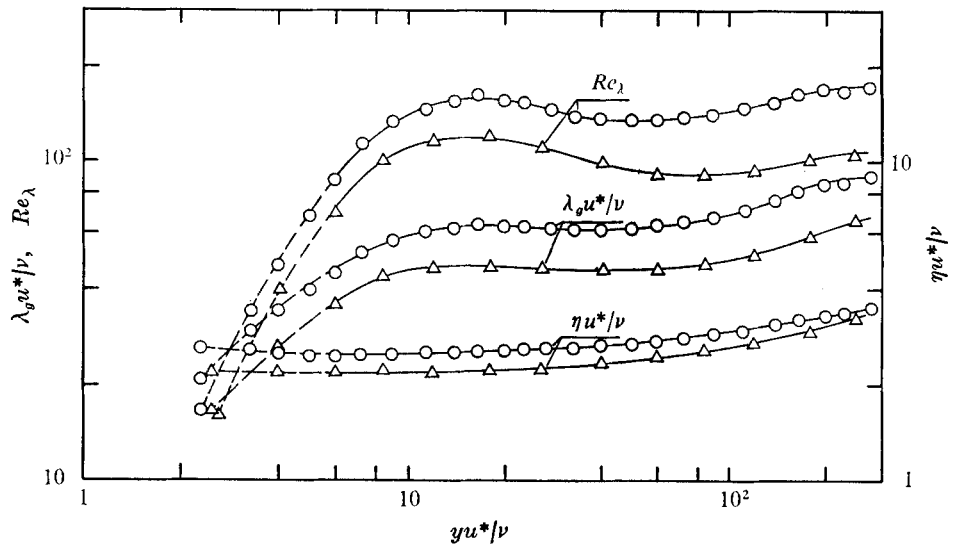

FIGURE 4. Distributions of Re_λ, the non-dimensional dissipation length scale λ_g^+ and the non-dimensional Kolmogorov microscale η^+. Re_δ: △, 11450; ○, 35500.

if there is still a finite probability for large amplitudes of e. At the same time $\mathscr{P}(e)$ then must be much more peaked than the $\mathscr{P}(e)$ of a signal with almost zero probability for a large amplitude. As Batchelor & Townsend (1949) pointed out, a peaked probability density with a long skirt means that the signal *must* show periods of relative silence, i.e. must show an intermittent character. Consequently a small value of the intermittency factor, defined as the fraction of time that turbulence occurs, yields a large value of the flatness factor. A large value of the flatness factor does not necessarily imply intermittency, however (Kuo & Corrsin 1971). For a normal probability density the intermittency factor $\gamma = 3{\cdot}0$. On the assumption of such a probability density during periods of high activity Batchelor & Townsend (1949) suggested determining the value of the flatness factor from $F = 3{\cdot}0/\gamma$.

The noise level of a compensated hot-wire signal increases linearly with frequency, while the energy spectrum of turbulence decreases rapidly with increasing frequency. Therefore, the signal-to-noise ratio is reduced at high frequency. Differentiation accentuates the high frequency component, so it tends to reduce the signal-to-noise ratio. Since the noise has approximately a normal probability density, the flatness factor tends to level off to 3·0 with decreasing signal-to-noise ratio. Therefore, a low-pass filter is used to cut off the highest frequency. The measured flatness factor increases with increasing high cut-off frequency and tends to approach a constant value at about the Kolmogorov frequency ($f_K = U/2\pi\eta$). At much higher cut-off frequencies, the signal-to-noise ratio decreases and the flatness factor levels off. This general tendency is the same as that suggested by Kuo & Corrsin (1971).

Following these authors, the Kolmogorov frequency was chosen as the high cut-off frequency. The distributions across the inner part of the wall region of the flatness factor of u and of its first and second derivatives are shown in figure 5.

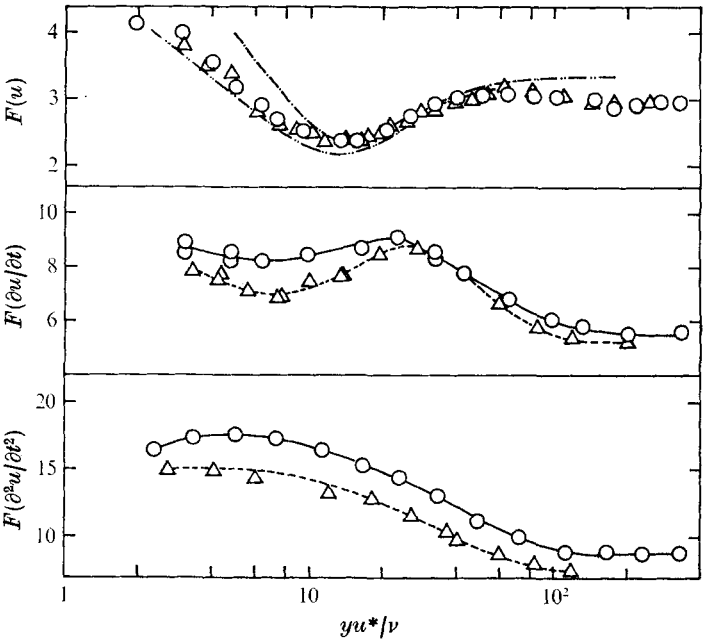

FIGURE 5. Distributions of the flatness factors of u, $\partial u/\partial t$ and $\partial^2 u/\partial t^2$. Re_δ: △, 11450; ○, 35500. –·–, Zarić (1972); –··–, Kreplin (1973).

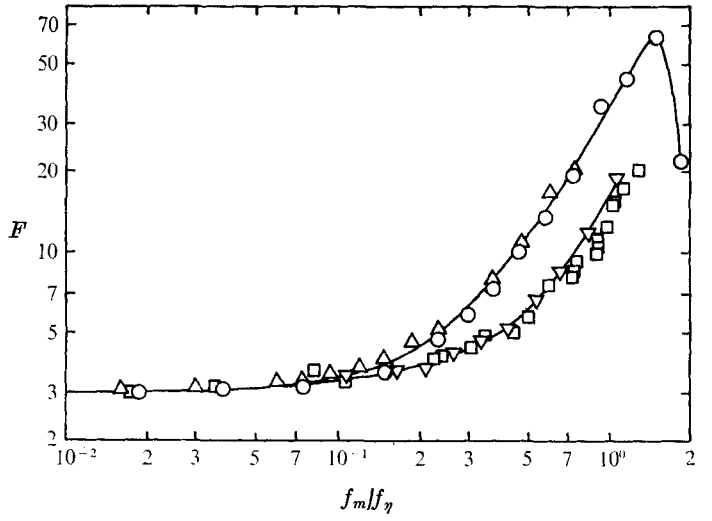

FIGURE 6. Flatness factor of band-pass signal as a function of the mid-band frequency f_m for a fixed relative bandwidth $\Delta f/f_m = 0{\cdot}24$. $Re_\delta = 35500$. y^+: ○, 5·01; △, 21·0; ▽, 332. □, Kuo & Corrsin (1971) for grid-produced turbulence at $Re_\lambda = 110$ and 86·5 with $\Delta f/f_m = 0{\cdot}52$.

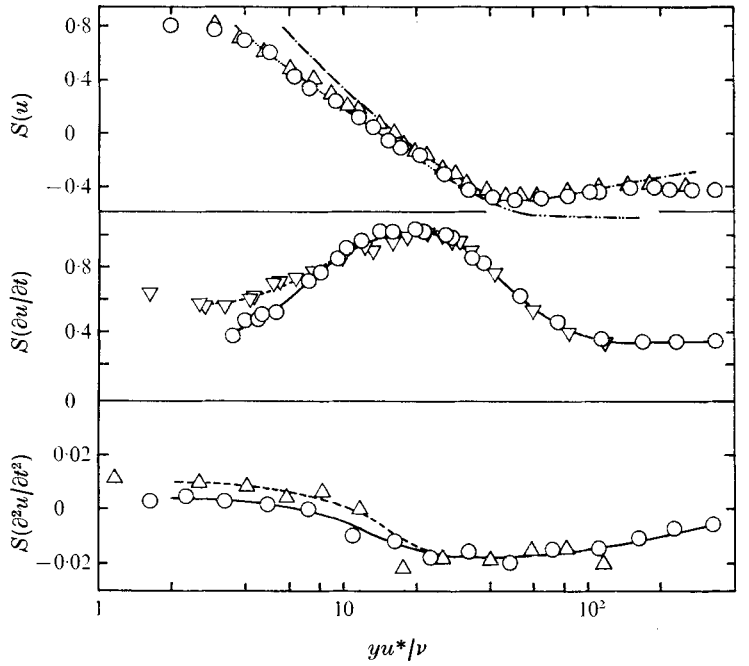

FIGURE 7. Distributions of skewness factors of u, $\partial u/\partial t$ and $\partial^2 u/\partial t^2$. Re_δ: △, ▽, 11450; ○, 35500. – · –, Zarić (1972); – ·· –, Kreplin (1973).

The flatness factor of band-pass signals with fixed relative bandwidth was measured and is shown in figure 6 as a function of mid-band frequency.

3.4. *Skewness factor*

The skewness factor is defined as

$$S(e) = \overline{e^3}/(\overline{e^2})^{\frac{3}{2}} = \int_{-\infty}^{\infty} de\, e^3 \mathscr{P}(e) \Big/ \left[\int_{-\infty}^{\infty} de\, e^2 \mathscr{P}(e)\right]^{\frac{3}{2}}. \tag{8}$$

Since the skewness factor is an odd-order moment of the probability density, it is an indication of the degree of asymmetry of $\mathscr{P}(e)$.

The effect of a high cut-off frequency on the skewness factors of u, $\partial u/\partial t$ and $\partial^2 u/\partial t^2$ is not so large as its effect on flatness factors. But in order to be consistent the Kolmogorov frequency has been set as the high cut-off frequency for all the data. Measured distributions of the skewness factors of u, $\partial u/\partial t$ and $\partial^2 u/\partial t^2$ are shown in figure 7.

3.5. *Spectra of non-negative random variables*

The spectra of $(\partial u/\partial t)^2$ and $(\partial^2 u/\partial t^2)^2$ are of special interest when studying the fine structure of turbulence. On the assumption of Taylor's hypothesis the probability distribution of $(\partial u/\partial x)^2$ and consequently that of the dissipation ϵ may be expected to be the same as that of $(\partial u/\partial t)^2$. According to Yaglom the variance of $(\partial u/\partial t)^2$ is given by (1) and its spectral distribution by (2). The spectra of $(\partial u/\partial t)^2$ and $(\partial^2 u/\partial t^2)^2$ measured at $Re_\delta = 35500$ are shown in figures 8 and 9,

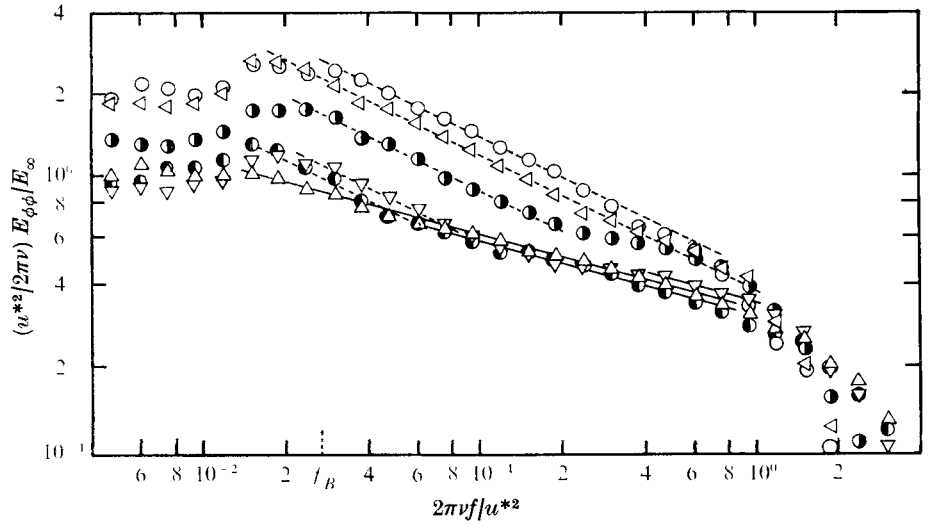

FIGURE 8. Change with y^+ of normalized spectral distribution $E_{\phi\phi}$ for $\phi = (\partial u/\partial t)^2$. $Re_\delta = 35500$. y^+: ○, 3·00; ◁, 5·00; ◑, 9·20; ▽, 21·0; ◐, 120; △, 334. Slope of solid lines = −0·276, slope of dashed lines = −0·500.

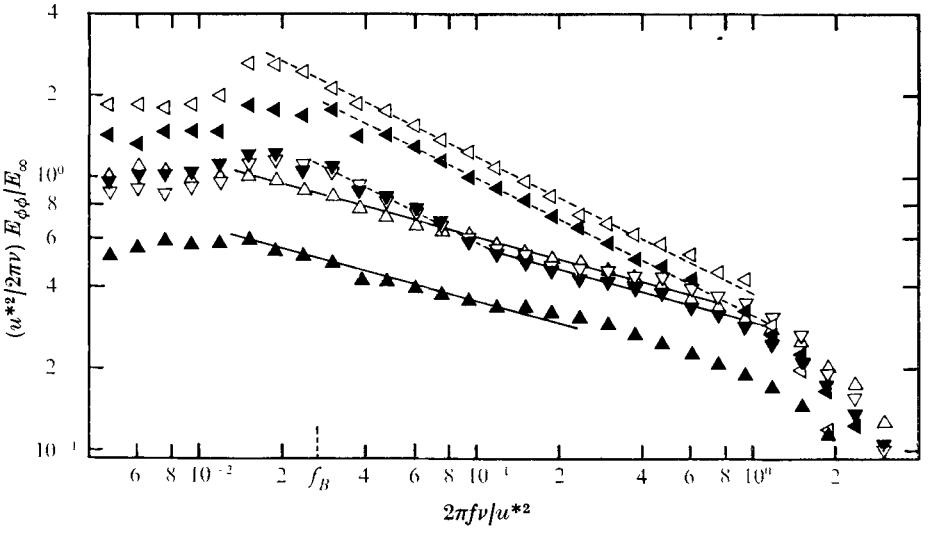

FIGURE 9. Comparison of normalized spectral distributions $E_{\phi\phi}$ for $\phi = (\partial u/\partial t)^2$ (open symbols) and for $\phi = (\partial^2 u/\partial t^2)^2$ (filled symbols). $Re_\delta = 35500$. y^+: ◁, 5·00; ▽, 21·0; △, 334.

with y^+ as a parameter. Note the increase of the frequency range with increasing distance from the wall. Figure 10 shows these spectra measured at three different Reynolds numbers and at two distances from the wall. For comparison one-dimensional spectra of u also measured at $Re_\lambda = 35500$ are shown in figure 11. At $y^+ = 334$ ($Re_\lambda \simeq 150$) a Kolmogorov inertial subrange is noticeable, while in the viscous sublayer the spectra clearly show a -1 power law in the lower frequency range. When comparing figure 11 with figures 8–10, note the more

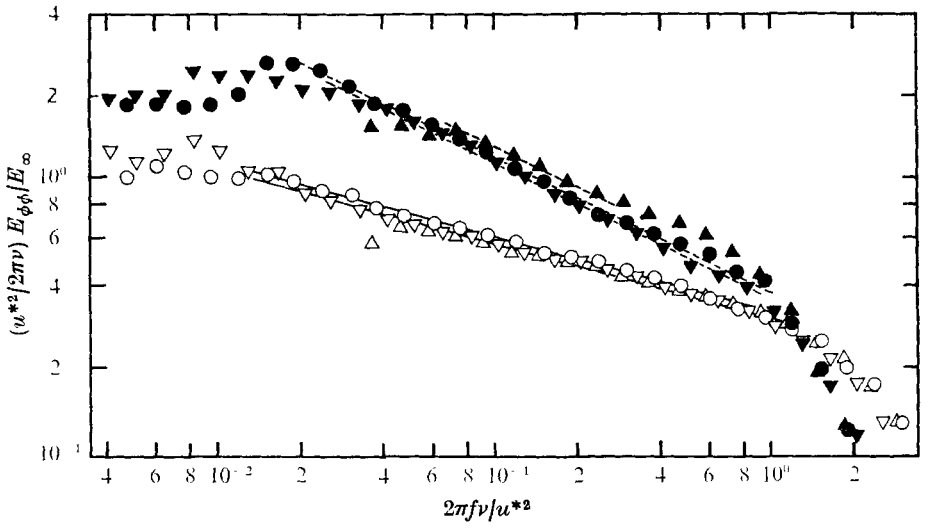

FIGURE 10. Comparison of normalized spectral distributions $E_{\phi\phi}$ for $\phi = (\partial u/\partial t)^2$ obtained at different Reynolds numbers. Re_δ: △, 11450; ○, 35500; ▽, 49200. Open symbols, $y/\delta = 0{\cdot}25$; filled symbols, $y^+ = 5{\cdot}0$.

extended frequency range for the spectra of $(\partial u/\partial t)^2$ and $(\partial^2 u/\partial t^2)^2$. The spectral distributions $E_{\phi\phi}$, where $\phi = u$, $(\partial u/\partial t)^2$ and $(\partial^2 u/\partial t^2)^2$ respectively, have been plotted in the following normalized and non-dimensional form:

$$\frac{u^{*2}}{2\pi\nu}\frac{E_{\phi\phi}}{E_\infty} \quad \text{where} \quad E_\infty = \int_0^\infty df E_{\phi\phi}.$$

4. Discussion

When considering in § 3.2 the results shown in figure 4, we mentioned possible errors made in calculating the dissipation $\bar{\epsilon}$ by assuming the isotropic relation (5) also to be applicable in the buffer region and viscous sublayer. Actually the dissipation may be expected to be greater there, and consequently the values of λ_g^+, Re_λ and η^+ calculated with the relation (5) are too high. Since $\eta \propto \bar{\epsilon}^{-\frac{1}{4}}$, the error in the determination of η may be less serious, though. From measurements of four out of the nine derivations occurring in (4), Laufer obtained $\bar{\epsilon}\nu/u^{*4}$ as a function of y^+. It showed a maximum equal to roughly 0·27 at $y^+ \simeq 8$. For smaller values of y^+ the variation of $\bar{\epsilon}\nu/u^{*4}$ with y^+ was practically linear according to

$$\bar{\epsilon}\nu/u^{*4} = 0{\cdot}1 + 0{\cdot}03y^+. \tag{9}$$

With this relation we obtain

$$\eta^+ = (0{\cdot}1 + 0{\cdot}03y^+)^{-\frac{1}{4}}, \tag{10}$$

with a limiting value of $\eta^+ = 1{\cdot}78$ when $y^+ \to 0$. This value for η^+ agrees reasonably with the value obtained from

$$\bar{\epsilon} = \nu[\overline{(\partial u/\partial y)^2} + \overline{(\partial w/\partial y)^2}] \quad \text{for} \quad y = 0.$$

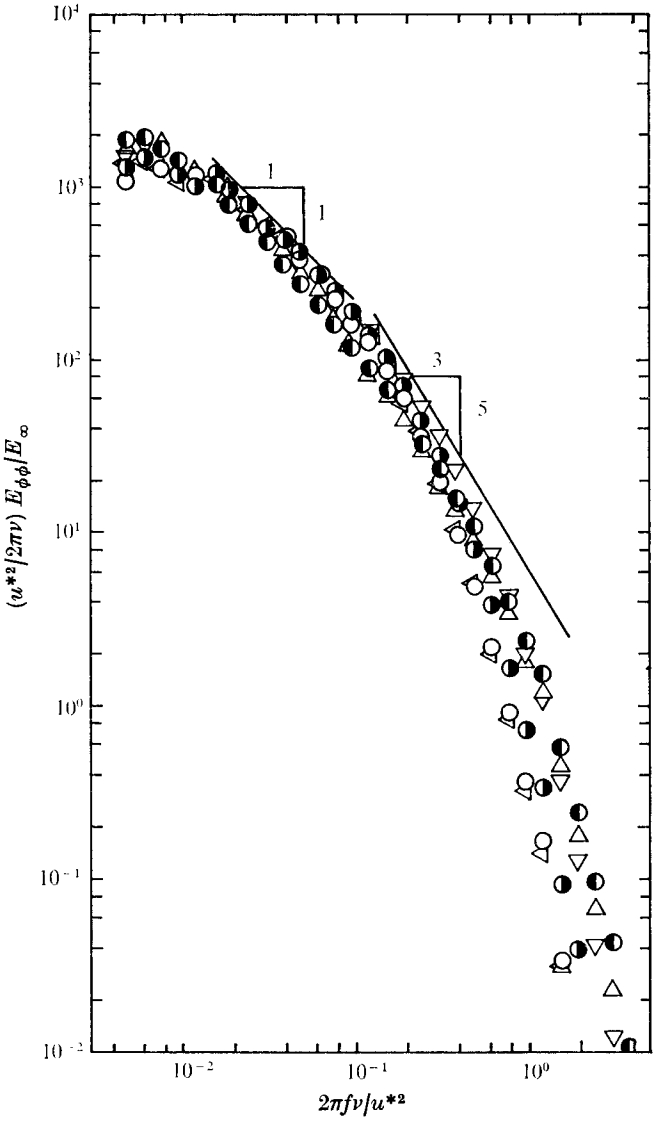

FIGURE 11. Normalized spectral distribution $E_{\phi\phi}$ for $\phi = u$. $Re_\delta = 35\,500$. y^+: ○, 3·00; ◁, 5·00; ◑, 9·20; ▽, 21·0; ◐, 120; △, 334.

From experiments by Eckelmann (1970) one concludes that $u'/u^* \simeq 0{\cdot}25y^+$ for $y^+ \to 0$. Since experimental evidence has shown that $u'/w' \simeq 3$ for $y^+ \to 0$, a limiting value of 1·95 is obtained for η^+. These two estimated values of η^+ are smaller than would be obtained from extrapolation of the experimental results shown in figure 4.

If one still defined λ_g by (5), with (9) one would obtain

$$\lambda_g^+ = \frac{u'}{u^*}\left(15\frac{u^{*4}}{\bar{\epsilon}\nu}\right)^{\frac{1}{2}} = \frac{u'}{u^*}\left(\frac{15}{0{\cdot}1 + 0{\cdot}03y^+}\right)^{\frac{1}{2}} \tag{11}$$

and consequently

$$Re_\lambda = \frac{u'^2}{u^{*2}} \left(\frac{15}{0{\cdot}1 + 0{\cdot}03y^+} \right)^{\frac{1}{2}}. \tag{12}$$

With $u'/u^* \simeq 0{\cdot}25y^+$ we then obtain for small y^+ the relations $\lambda_g^+ \simeq 3{\cdot}1y^+$ and $Re_\lambda \simeq 0{\cdot}75y^+$, which clearly yield much smaller values of λ_g^+ and Re_λ than would be obtained from figure 4.

The flatness and the skewness factors of u, $\partial u/\partial t$ and $\partial^2 u/\partial t^2$ determined at the two Reynolds numbers and shown in figures 5 and 7 fall roughly on a single curve, thus pointing to the existence of Reynolds number similarity.

Frenkiel & Klebanoff (1967) and Van Atta & Chen (1968) measured the flatness and skewness factors of the u signal using a digital method. They discussed the nonlinearity effect of the hot-wire response and the low frequency cut-off effect, and found that these effects are serious in the case of the odd-order moments of u. Van Atta & Chen then showed that if these effects are taken into account the values of the flatness and the skewness factor in grid-produced turbulence are three and zero respectively, within the experimental accuracy. If we too take into account the possible errors due to these effects and also due to the analog method used here, we may expect from the figures 5 and 7 that the flatness and skewness factors of u may be regarded as having the values three and zero in the outer part of the wall region, $y^+ > 100$. Thus in this part the u fluctuation has a normal probability distribution. In the region $y^+ < 15$, the skewness factor becomes positive and increases with decreasing y^+. At approximately $y^+ = 15$ the flatness factor of u has a minimum, while the skewness factor becomes zero. This location agrees with that where u'/u^* reaches a maximum (figure 3) and where, according to experimental evidence, the highest turbulence production occurs. The agreement of these results with those obtained by Kreplin (1973) and by Zarić (1972), which were obtained with the digital method, is satisfactory. This gives strong support to the reliability of the analog method used here.

For the digital data for the $\partial u/\partial t$ signal obtained in grid-produced turbulence Frenkiel & Klebanoff (1971) estimated the nonlinear effect on moments of this signal up to the sixth order, and found it to be negligible. Therefore, although the relative intensity of the turbulence is large in the wall region, this effect, as well as the low frequency cut-off effect, is not expected to be very significant for the data for the first and second velocity derivative obtained here.

As shown in figure 7, the skewness factor of $\partial u/\partial t$ is also not zero, but has a large positive value with a flat maximum at roughly $y^+ = 20$. The absolute value of the skewness factor of $\partial^2 u/\partial t^2$ is smaller by two orders of magnitude than that of $\partial u/\partial t$, and may be regarded as zero. This is in agreement with results obtained by Stewart & Townsend (1951) in a grid-produced turbulence and by Wyngaard & Tennekes (1970) in a curved mixing layer. In figure 7 the skewness factors of u, $-\partial u/\partial t$ (or $\partial u/\partial x$) and $\partial^2 u/\partial t^2$ (or $\partial^2 u/\partial x^2$) all decrease with increasing y^+ and have a minimum in the buffer region. After rising again they gradually approach constant values.

The skewness and flatness factors of $\partial u/\partial t$ as a function of Re_λ obtained in our investigation at $y/\delta = 0{\cdot}25$ are compared in figures 12(a) and (b) with those

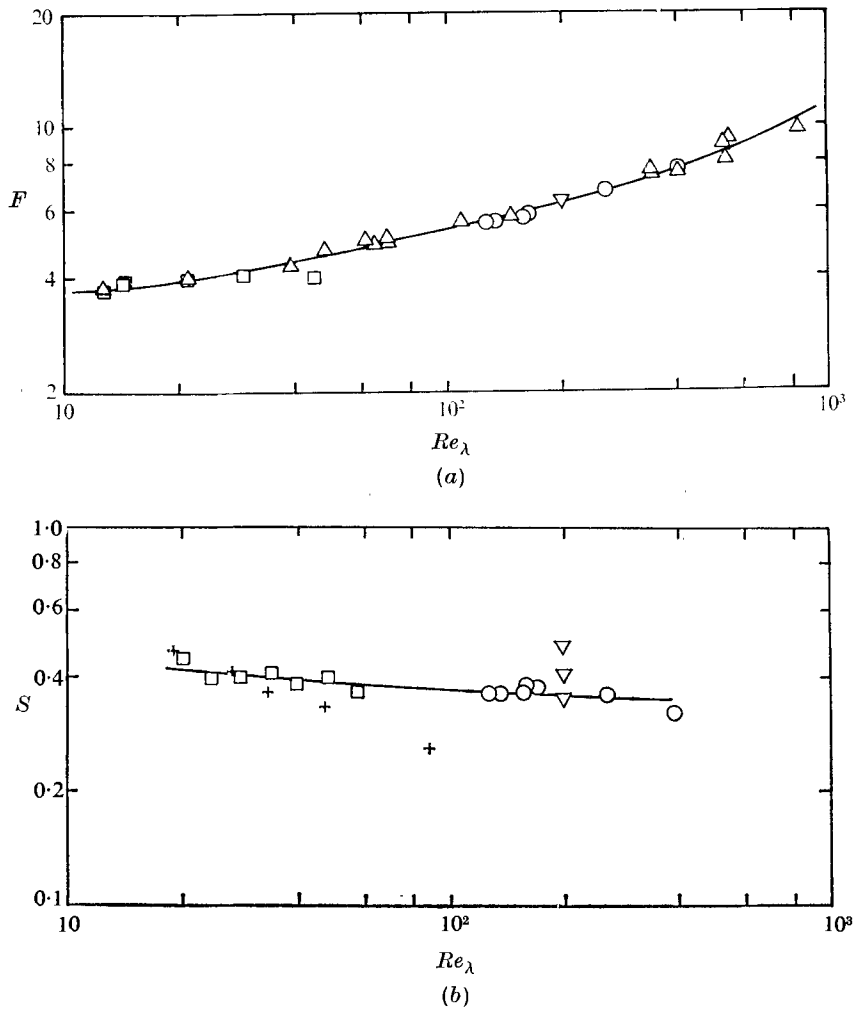

FIGURE 12. (*a*) Flatness factor F and (*b*) skewness factor S of $\partial u/\partial t$ as a function of Re_λ. ○, measurements at $y/\delta = 0{\cdot}25$; □, Batchelor & Townsend (1949); +, Stewart & Townsend (1951); ▽, Wyngaard & Tennekes (1970); △, Kuo & Corrsin (1971).

obtained by Batchelor & Townsend (1949), Stewart & Townsend (1951), Wyngaard & Tennekes (1970) and Kuo & Corrsin (1971) in unsheared flows, namely in grid-produced turbulence and on the axes of a turbulent jet and a turbulent wake. The agreement is satisfactory.

Also our measured values of the flatness factor of $\partial^2 u/\partial t^2$ appear to compare well with Kuo & Corrsin's results for this quantity. Consequently, it may be concluded that in the outer part of the wall region ($y^+ > 100$) the flatness and skewness factors tend to approach those values which are obtained in shear-free turbulence at the same Re_λ.

Although Re_λ is almost constant in the region $20 < y^+ < 100$, the flatness factors of both $\partial u/\partial t$ and $\partial^2 u/\partial t^2$ increase with decreasing y^+. For $y^+ < 20$ the

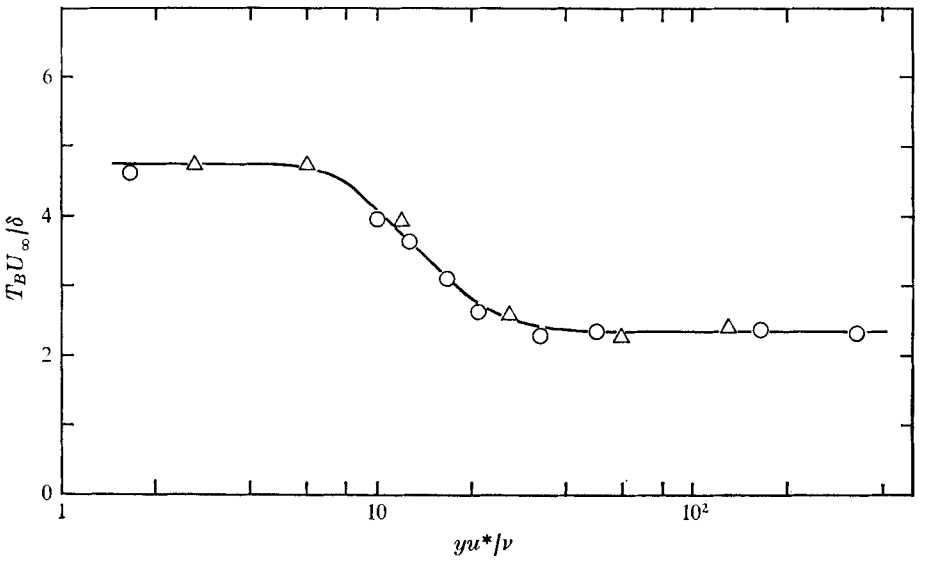

FIGURE 14. Distribution of burst period T_B of band-pass signal ($f_m = 0{\cdot}5f_\eta$). Re_δ: △, 11450; ○, 35500.

flatness factor of $\partial^2 u/\partial t^2$ continues to increase though Re_λ decreases there with decreasing y^+. In the viscous sublayer it attains a value about twice the value observed in the outer part of the wall region. If we connect the value of the flatness factor with the intermittent inrush and ejection processes, the above behaviour of the flatness factor strongly suggests that these processes affect different regions of the flow. While the flow in the outer part is influenced by both the inrush and ejection events, the flow in the vicinity of the wall is affected mainly by the inrush event ($\partial u/\partial t > 0$). This is supported by the character of the oscillograms of $\partial u/\partial t$ in figure 13(*a*) (plate 1), which shows a sequence of positive pulses in the innermost part of the wall region. By comparing the oscillograms of u and $\partial u/\partial t$, it may be concluded that these positive pulses may be considered to be associated with the inrush of high momentum fluid lumps into the inner layer. This large influence of the inrush phase is reflected in the remarkably large positive value of the skewness factor of $\partial u/\partial t$.

Rao, Narasimha & Badra Narayanan (1971) counted the burst rate of the high frequency band-pass signal of the u fluctuation and related it to the period of the inrush–ejection cycle. In their experiment, which was made in the region $y^+ > 30$, bursts of high frequency components occurred twice in each cycle. On the average, a burst occurred once in the inrush phase and once in the ejection phase. In figure 13 bursts of high frequency components (mid-band frequency $f_m = 0{\cdot}5f_\eta$) are clearly visible. By counting these bursts in a similar way to Rao *et al.*, the period of the inrush–ejection cycle was obtained. Figure 14 shows that the period of the inrush–ejection cycle non-dimensionalized by the outer parameters U_∞ and δ, i.e. $T_B U_\infty/\delta$, is 4·7. It does not depend on the Reynolds number, which agrees well with the results of Rao *et al.* (1971).

In the inner part of the wall region bursts due to ejection ($\partial u/\partial t < 0$) tend to diminish as the wall is approached and in the viscous sublayer a burst occurs once in each cycle (figure 13(*a*) and figure 14). This results in a small intermittency factor and in a high flatness factor for the fine structure of the turbulence in that layer. One piece of evidence is clearly shown in figure 6. The distribution of the flatness factor of the band-pass signal *vs.* mid-band frequency changes as the distance yu^*/ν is increased. The flatness factor in and near the viscous sublayer becomes about twice that in the outer part in the high frequency region when $f_m/f_\eta > 0{\cdot}45$. This is expected, if we may assume that inrush and ejection phases make the same contribution to the flatness factor in the outer part, while the contribution of the ejection phase diminishes in the viscous sublayer.

The distribution of this flatness factor at $y^+ = 332$ as a function of f_m/f_η is in good agreement with the result obtained by Kuo & Corrsin (1971) in nearly isotropic turbulent flow. This is another confirmation of the idea that the fine structure of the turbulence in the outer part is substantially the same as that in isotropic turbulent flow.

The change in the mechanism of the fine structure of the turbulence with the distance from the wall is clearly shown by the spectra of $(\partial u/\partial t)^2$ and $(\partial^2 u/\partial t^2)^2$. In the outer part the spectrum of $(\partial u/\partial t)^2$ shows a power-law behaviour over more than two decades (figure 8). It covers almost the entire frequency range of the turbulent energy spectrum (figure 11). This is worth noting since Yaglom's model was derived on the assumption of a very high Reynolds number and has to be applied to the restricted frequency region of the inertial subrange. In spite of the Yaglom assumption, the power law appears to persist in the measured spectra in the range from the region where the frequency is less than that of energy-containing eddies to that in which molecular viscosity begins to affect the spectrum. In the viscous sublayer a power law can again be observed clearly but with a different exponent. This power law applies also to a large part of the whole frequency range of the energy spectrum, with the exception of the highest viscous frequency range. From the spectra in the buffer region we can see how the change in the spectrum occurs with increasing y^+. In the spectrum there are two distinct power-law regions (figures 8 and 9). In the lower frequency region the power is the same as that for the viscous sublayer, while in the high frequency region it is the same as that for the outer part of the wall region. As y^+ increases, the range of the power law for the higher frequency region increases to lower frequencies till it covers the whole frequency range.

Yaglom assumed for the inertial subrange an exponent equal to $\mu - 1$ [see (3)] with a value of μ between 0 and 1. However, the present experiments show that it depends on the distance from the wall. This is not surprising since close to the wall the energy spectra hardly show an inertial subrange (see figure 11). The values of μ obtained in the present experiments are compared with those of other investigators in table 2.

With a burst period given by $T_B U_\infty/\delta = 4{\cdot}7$ one obtains for the main burst frequency f_B expressed in terms of the wall variables u^* and ν the value

$$2\pi f_B = 2{\cdot}7 \times 10^{-2} u^{*2}/\nu$$

Investigators	Quantity	μ		
Gurvich & Zubkovski (1963)	$(\partial w/\partial t)^2$	0·4	$y = 4\,\mathrm{m}$	Wind blowing over the ground
Pond & Stewart (1965)	$(\partial u/\partial t)^2$	0·4	$y = 1\,\mathrm{m}$	Wind blowing over the water
	$[(\partial u/\partial t)^{\sim}]^2$†	0·6		
Gurvich & Yaglom (1967)	$(\partial T/\partial t)^2$	0·4		Wind blowing over the ground
Van Atta & Chen (1970)	$(\partial u/\partial t)^2$	0·5	$y = 31\,\mathrm{m}$	Wind blowing over the open ocean
Wyngaard & Tennekes (1970)	$(\partial u/\partial t)^2$	0·85		Curved mixing-layer flow, $Re_\lambda = 200$
Sheih *et al.* (1971)	$(\partial u/\partial t)^2$	0·7	$y = 108\,\mathrm{m}$	Wind blowing over the ground
Present authors	$(\partial u/\partial t)^2$	0·724	$yu^*/\nu = 320$	Turbulent boundary-layer flow, $\mathrm{Re}_\theta = 1244$ and 4248
		0·500	$yu^*/\nu < 5$	
	$(\partial^2 u/\partial t^2)^2$	0·765	$yu^*/\nu = 320$	
		0·500	$yu^*/\nu < 5$	

† Specially averaged value of $\partial u/\partial t$ employing a special filter.

TABLE 2. Experimental values of the coefficient μ

at $Re_\delta = 35\,500$. This burst frequency is indicated in figures 8 and 9. It may be noted that the above power law for the viscous sublayer begins roughly at this frequency.

The same phenomena may be observed in the spectra of $(\partial^2 u/\partial t^2)^2$. Both in the outer layer and in the viscous sublayer the spectra decrease with frequency according to a power law but with different exponents (figure 9). The values of μ are 0·765 and 0·500 for the outer layer and for the viscous sublayer respectively, which compare well with values of 0·724 and 0·500 for the spectra of $(\partial u/\partial t)^2$. When the spectra of $(\partial u/\partial t)^2$ and $(\partial^2 u/\partial t^2)^2$ measured in the buffer layer

$$(yu^*/\nu = 21{\cdot}0)$$

are compared, it is noticed that the critical frequency at which transition occurs from the power law ($\mu = 0{\cdot}500$) is almost the same. Therefore, the spectra of $(\partial u/\partial t)^2$ and $(\partial^2 u/\partial t^2)^2$ agree with each other within the experimental error at all distances from the wall.

Our thanks are due to the Delfts Hogeschoolfonds for granting to H. Ueda a research fellowship during the period 1972–1973. One of the authors (H.U.) would like to thank Prof. T. Mizushina of Kyoto University for his valuable suggestions and continued interest in this study. Kyoto University and the Kawakami Memorial Foundation both contributed through grant support and assigned research.

REFERENCES

BATCHELOR, G. K. & TOWNSEND, A. A. 1949 *Proc. Roy. Soc.* A **199**, 238.

CORINO, E. R. & BRODKEY, R. S. 1969 *J. Fluid Mech.* **37**, 1.

ECKELMANN, H. 1970 *Mitteilungen Max-Planck-Institut für Strömungsforschung und Aerodynamische Versuchsanstalt, Göttingen*, no. 48.

FRENKIEL, F. N. & KLEBANOFF, P. S. 1967 *Phys. Fluids*, **10**, 1737.

FRENKIEL, F. N. & KLEBANOFF, P. S. 1971 *J. Fluid Mech.* **48**, 183.
GIBSON, C. H., STEGEN, G. H. & WILLIAMS, R. B. 1970 *J. Fluid Mech.* **41**, 153.
GRASS, A. J. 1971 *J. Fluid Mech.* **50**, 233.
GURVICH, A. S. & YAGLOM, A. M. 1967 *Phys. Fluids*, **10** (suppl.), 559.
GURVICH, A. S. & ZUBKOVSKI, S. L. 1963 *Izv. Akad. Nauk S.S.S.R., Ser. Geophys.* no. 1856.
HINZE, J. O. 1959 *Turbulence*. McGraw-Hill.
HINZE, J. O. 1973 *Appl. Sci. Res.* **28**, 453.
KIM, H. T., KLINE, S. J. & REYNOLDS, W. C. 1971 *J. Fluid Mech.* **50**, 133.
KLEBANOFF, P. S. 1955 *N.A.C.A. Tech. Rep.* no. 1247.
KLINE, S. J., REYNOLDS, W. C., SCHRAUB, F. A. & RUNDSTADLER, P. W. 1967 *J. Fluid Mech.* **30**, 741.
KOLMOGOROV, A. N. 1941 *C. R. Acad. Sci. (Dokl.) U.S.S.R.* **30**, 301.
KOLMOGOROV, A. N. 1962 *J. Fluid Mech.* **13**, 81.
KREPLIN, H. P. 1973 M.Sc. thesis, Max-Planck-Institut für Strömungsforschung.
KUO, A. Y. S. & CORRSIN, S. 1971 *J. Fluid Mech.* **50**, 285.
KUO, A. Y. S. & CORRSIN, S. 1972 *J. Fluid Mech.* **56**, 447.
LAUFER, J. 1953 *N.A.C.A. Tech. Note*, no. 2954.
LAUFER, J. 1954 *N.A.C.A. Tech. Rep.* no. 1174.
LAWN, C. J. 1971 *J. Fluid Mech.* **48**, 477.
LUDWIEG, H. & TILLMANN, W. 1949 *Ing. Arch.* **17**, 288.
MORRISON, W. R. B. & KRONAUER, R. E. 1969 *J. Fluid Mech.* **39**, 117.
NIKURADSE, J. 1933 *V.D.J. Forschungsheft*, no. 361.
OBOUKHOV, A. M. 1962 *J. Fluid Mech.* **13**, 77.
ORSZAG, S. A. 1970 *Phys. Fluids*, **13**, 2211.
PAO, Y. H. 1965 *Phys. Fluids*, **8**, 1063.
PATEL, V. C. 1965 *J. Fluid Mech.* **23**, 185.
POND, S. & STEWART, R. W. 1965 *Izv. Acad. Sci. U.S.S.R., Atmos. Oceanic Ser.* **1**, 914.
RAO, K. N., NARASIMHA, R. & BADRI NARAYANAN, M. A. 1971 *J. Fluid Mech.* **48**, 339.
SANDBORN, V. A. 1959 *J. Fluid Mech.* **6**, 211.
SCHLICHTING, H. 1968 *Boundary Layer Theory*. McGraw-Hill.
SHEIH, C. W., TENNEKES, H. & LUMLEY, J. L. 1971 *Phys. Fluids*, **14**, 201.
STEWART, R. W. & TOWNSEND, A. A. 1951 *Phil. Trans.* A **243**, 359.
STEWART, R. W., WILSON, J. R. & BURLING, R. W. 1970 *J. Fluid Mech.* **41**, 141.
TENNEKES, H. & WYNGAARD, J. C. 1972 *J. Fluid Mech.* **55**, 93.
VAN ATTA, C. W. & CHEN, W. Y. 1968 *J. Fluid Mech.* **34**, 497.
VAN ATTA, C. W. & CHEN, W. Y. 1970 *J. Fluid Mech.* **44**, 145.
WALLACE, J. M., ECKELMANN, H. & BRODKEY, R. S. 1972 *J. Fluid Mech.* **54**, 39.
WILLMARTH, W. W. & LU, S. S. 1972 *J. Fluid Mech.* **55**, 65.
WILLS, J. A. B. 1962 *J. Fluid Mech.* **12**, 388.
WYNGAARD, J. C. 1968 *J. Sci. Instrum.* (*J. Phys.* E), **1** (2), 1105.
WYNGAARD, J. C. & COTÉ, O. R. 1971 *J. Atmos. Sci.* **28**, 190.
WYNGAARD, J. C. & TENNEKES, H. 1970 *Phys. Fluids*, **13**, 1962.
YAGLOM, A. M. 1966 *Sov. Phys. Dokl.* **11**, 26.
ZARIĆ, Z. 1972 *4th All-Union Heat Mass Transfer Conf., Minsk, U.S.S.R.*

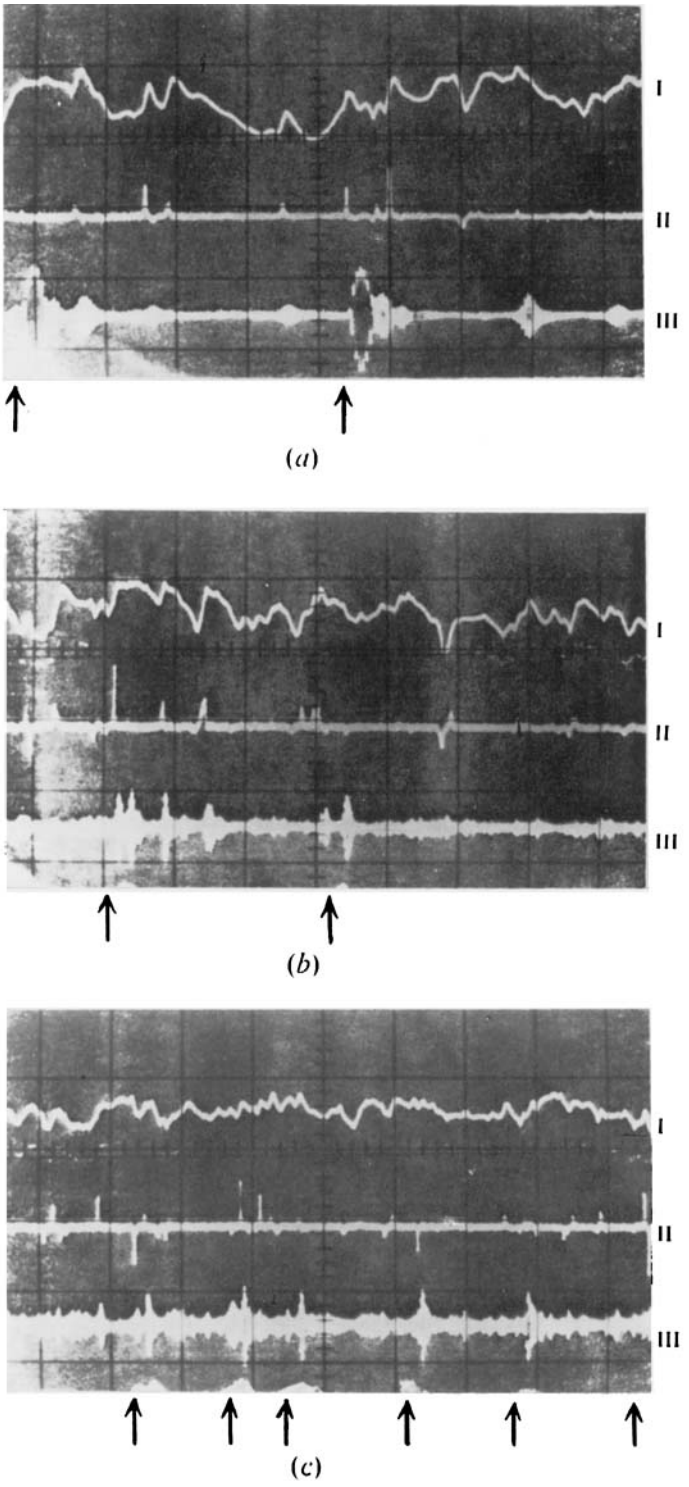

FIGURE 13. Oscillograms of (I) $u(t)$ signal, (II) $(\partial u/\partial t)^3$ signal and (III) band-pass signal. Mid-band frequency $f_m = 0{\cdot}5\, f_\eta$. Bandwidth $\Delta f/f_m = 0{\cdot}24$; i.e. 0·02 s/division. $Re_\delta = 11\,450$. (*a*) $y^+ = 5{\cdot}01$; (*b*) $y^+ = 17{\cdot}9$; (*c*) $y^+ = 159$.